Available online at www.sciencedirect.com

ScienceDirect

Ceramics International 40 (2014) 7971–7982

CERAMICS INTERNATIONAL

www.elsevier.com/locate/ceramint

In-vitro corrosion inhibition mechanism of fluorine-doped hydroxyapatite and brushite coated Mg–Ca alloys for biomedical applications

H.R. Bakhsheshi-Rad[a,*], E. Hamzah[a], M. Daroonparvar[a], R. Ebrahimi-Kahrizsangi[b], M. Medraj[c]

[a]Department of Materials Engineering, Faculty of Mechanical Engineering, Universiti Teknologi Malaysia, 81310 Johor Bahru, Johor, Malaysia
[b]Materials Engineering Department, Najafabad Branch, Islamic Azad University, Najafabad, Isfahan, Iran
[c]Department of Mechanical Engineering, Concordia University, 1455 De Maisonneuve Blvd. West, Montreal, QC H3G 1M8, Canada

Received 13 November 2013; received in revised form 25 December 2013; accepted 28 December 2013
Available online 7 January 2014

Abstract

Magnesium alloys have received great attention as a new kind of biodegradable metallic biomaterials. However, they suffer from poor corrosion resistance. In this study, Mg–Ca alloy was coated with nano-fluorine-doped hydroxyapatite (FHA), and brushite (DCPD); via electrochemical deposition (ED). Coatings were characterized by X-ray diffraction (XRD), Fourier-transformed infrared spectroscopy (FTIR), transmission electron microscopy (TEM), scanning electron microscopy (SEM) and energy dispersive X-ray spectroscopy (EDS). The results revealed that nano-fluorine-doped hydroxyapatite coating produced more dense and uniform coating layer, compared to the brushite coating. The compression tests of the ED-coated Mg alloy samples immersed in simulated body fluid for different time periods showed higher yield strength (YS) and ultimate tensile strength (UTS), compared to those of the uncoated samples. The degradation behavior and corrosion properties of the ED-coated Mg alloy samples were examined via electrochemical measurements and immersion tests. The results showed that FHA coating could effectively induce the precipitation of more Ca^{2+} and PO_4^{3-} ions than DCPD coating, because the nanophase can provide higher specific surface area. It was also found that FHA and DCPD coatings can significantly decline the initial degradation rate of the alloy. A corrosion mechanism of the ED-coated alloy is proposed and discussed in this paper.

Keywords: C. Corrosion; C. Mechanical properties; D. Apatite; E. Biomedical applications

1. Introduction

Biodegradable implants are receiving huge attention in medical applications [1]. They are dissolved and absorbed in the human body after the healing process is complete [1,2]. In that regard, they are superior to permanent implants, since their presence in the human body may cause problems such as sensitization, physical irritation, allergy and/or other physical problems in the long term. Equally, the patient′s morbidity and overall cost can be reduced, significantly, by using degradable implants; since there is no need for extra surgery for their removal [2,3]. Recently, accessible degradable implants are mainly made of polymers or ceramics, such as poly-l-lactic acid, polyglycolic acid (PGA), polyglyconate and calcium phosphate ceramics [4,5]. However, polymeric materials possess lower mechanical strength, compared to metallic materials. Hence, these materials are mainly employed for low load-bearing applications [2]. Compared to the commonly used biodegradable materials, magnesium alloys show great potential for implant applications as a result of their outstanding mechanical properties, biocompatibility and non-toxicity [3,6].

Magnesium is a lightweight metal with a density of 1.74 g/cm^3, similar to that of natural bones (1.8–2.1 g/cm^3), and an elastic modulus of 44 GPa. The density of Mg is 1.6 and 4.5 times lower than that of aluminum and steel, respectively. Its elastic modulus is close to that of cortical bone (17 GPa), which results stress shielding effect [3,7,8]. In the human body, large amount of Mg^{2+} ions exist; taking part in several metabolic reactions [1]. However, the application of these materials has been limited due to their high corrosion rate and fast biodegradation before the adequate healing of the new tissue [9,10]. Several types of corrosion, such as galvanic and pitting corrosions, are observed in magnesium alloys [11].

*Corresponding author. Tel.: +60 147382258.
E-mail addresses: rezabakhsheshi@gmail.com, bhamidreza2@live.utm.my (H.R. Bakhsheshi-Rad).

0272-8842/$ - see front matter © 2014 Elsevier Ltd and Techna Group S.r.l. All rights reserved.
http://dx.doi.org/10.1016/j.ceramint.2013.12.147

The simplest way to reduce the corrosion rate of magnesium and its alloys is by coating, which acts as a protective layer against a corrosive environment [1,12]. To modify the surface of metal implants; bioactive coatings, such as various ceramic calcium phosphate (Ca–P) compounds, are promising candidates [13]. Brushite (DCPD, $CaHPO_4 \cdot 2H_2O$), and hydroxyapatite (HA, $Ca_{10}(PO_4)_6(OH)_2$) are two kinds of Ca–P coatings, which form a protective layer on Mg alloys to improve their biocompatibility and corrosion resistance [14]. Brushite crystals are composed of $CaPO_4$ chains, arranged parallel to each other, while lattice water molecules are interlayered among them [15]. Brushite also has biocompatibility with different cell lines such as murine fibroblast cells [16]. In medical field, it is used as calcium orthophosphate cements and for tooth remineralization [15]. Addition of brushite to toothpaste for caries prevention and as gentle polishing agent has also been reported [16]. However, brushite encounters higher solubility than other types of calcium phosphate phases. Thus, it is mainly applied as a precursor to synthesize the more stable HA phase. This is attributed to the modification of brushite crystal size via homogeneous precipitation, which can be easily converted to HA through alkaline treatment [16]. Similar approach was used by other researchers to convert brushite to calcium deficient hydroxyapatite (CDHA) using NaOH [15,16]. Hydroxyapatite is widely used as a bone implant material owing to its excellent biocompatibility and it can also form strong chemical bond with the bone [17,18]. HA can also be used as a coating material on biodegradable and permanent metallic implants due to its chemical and biological similarity to the natural bone [19,20]. The deposit of HA on the surface of magnesium alloys enhances bioactivity and improves both bone-bonding ability and corrosion resistance of these alloys [1]. However, HA coating suffers from relatively high dissolution rate in the biological environment of human body, which is unfavorable for long-term stability of the implants [17,19,21,22]. Therefore, recently, hydroxyapatite is doped with different quantities of cations and anions such as Na^+, Mg^{2+}, CO_3^{-2} and F^{-1} [23]. Among these, F^{-1} ion plays a crucial role owing to its effect on the physical and biological properties of hydroxyapatite. F^{-1} ion also prevents dental cavities in a bacteria containing and acidic environment. It equally acts as a good nucleation agent for apatite, which promotes bone forming process [24]. Therefore, FHA $(Ca_{10}(PO_4)_6\ (OH)_{2-x}F_x$, where $0 < x < 2$) was developed as a promising candidate for the replacement of HA in orthopedic applications [25]. FHA also shows high phase stability at higher temperatures due to the replacement of OH^- by F^- which leads to contraction in the *a*-axis without changing the *c*-axis. This causes an enhancement of the crystallinity and stability [17]. Different surface treatments, such as polymer coating, hydrothermal, chemical, sol–gel, electrochemical deposition, dip coating, anodizing and micro-arc oxidation (MAO) have been carried out on magnesium alloys for the enhancement of their corrosion resistance [11]. Among these, electrodeposition (ED) is a promising method for coating calcium phosphate on magnesium and its alloys owing to its simple set up, cost-effectiveness, ability to form a uniform coating, low temperature requirement and ability to coat complex shapes [26]. Other studies have also reported HA coating on Mg alloys via electrodeposition method [27]. However, the degradation mechanism of fluorine-doped hydroxyapatite coating on Mg alloys in simulated body fluid (SBF) is not yet understood. Therefore, in this study, the corrosion behavior of Mg–Ca alloy with FHA, and DCPD coatings in SBF was systematically evaluated. Mechanical properties dependence on the degradation behavior of the uncoated and DCPD, and FHA specimens were also investigated.

2. Experimental

Pure magnesium (99.98% Mg), pure zinc (99.99%) and Mg–32% Ca master alloy were used to prepare magnesium alloys. Melting was conducted in an electric resistance furnace under argon gas in a mild steel crucible coated with boron nitride. The melting temperature was set at 760 °C and the melt was kept for 45 min, at this temperature. The melt, with a constant concentration of Ca (3 wt%), was then cast into a stainless steel mold pre-heated to 300 °C to produce an ingot. In preparation for further experiments, several Mg–3% Ca specimens, with composition of 0.059% Si, 0.038% Mn, 3.271% Ca, 0.021% Al, 0.013% Fe and 96.598% Mg and dimensions of 20 mm × 15 mm × 10 mm, were cut from the ingot. Then, they were mechanically wet ground with 320–2000 SiC grit papers until all visible scratches were removed. Prior to a deposition, the polished specimens were washed thoroughly with distilled water, rinsed and ultrasonically degreased with ethanol and dried in a warm stream of air. Brushite coating was produced via electrodeposition, at 70 °C, for 1 h. A conventional cell was fitted with a graphite rod as the anode and an Mg–Ca sheet ($15 \times 15 \times 10\ mm^3$) as the cathode. Saturated calomel electrode (SCE) served as the reference electrode, along with a potentiostat/galvanostat instrument (VersaSTAT 3-VersaStudio software) for electrochemical measurements. A current density of 0.4 mA/cm^2 was used for the coating process. The solution concentration was kept uniform using a magnetic stirrer, controlled at 120 rpm. The electrolyte was prepared from the mixture of $Ca(NO_3)_2$ (0.042 mol/L), $NH_4H_2PO_4$ (0.025 mol/L), $NaNO_3$ (0.1 mol/L) and H_2O_2 (10 mol/L). The addition of $NaNO_3$ enhances the ionic strength. All of the aforementioned reagents were analytically graded. The pH value of the solution was adjusted to 5.0 by adding HNO_3 and $(CH_2OH)_3CNH_2$, at room temperature. The FHA coating was directly electrodeposited after adding NaF (2 mmol/L), at 60 ± 1 °C, into the electrolyte. The addition of 2 mmol/L of NaF into the electrolyte ensured a crystallized apatite structure in the FHA coating. An X-ray diffractometer (Siemens-D5000) was used to evaluate the phase transformation and crystallite size, using Cu-Kα radiation ($\lambda = 1.5405$ Å) generated at 35 kV and 25 mA. The crystallite size was determined by the following Scherer equation [25]:

$$t = 0.89k\lambda/\beta\ \cos\ \theta \quad (1)$$

where k is a form coefficient (assuming that in our case $k = 1$), β is the diffraction peak width at mid-height, λ is the X-ray wave length, t is the average crystallite size (nm) and θ is the Bragg

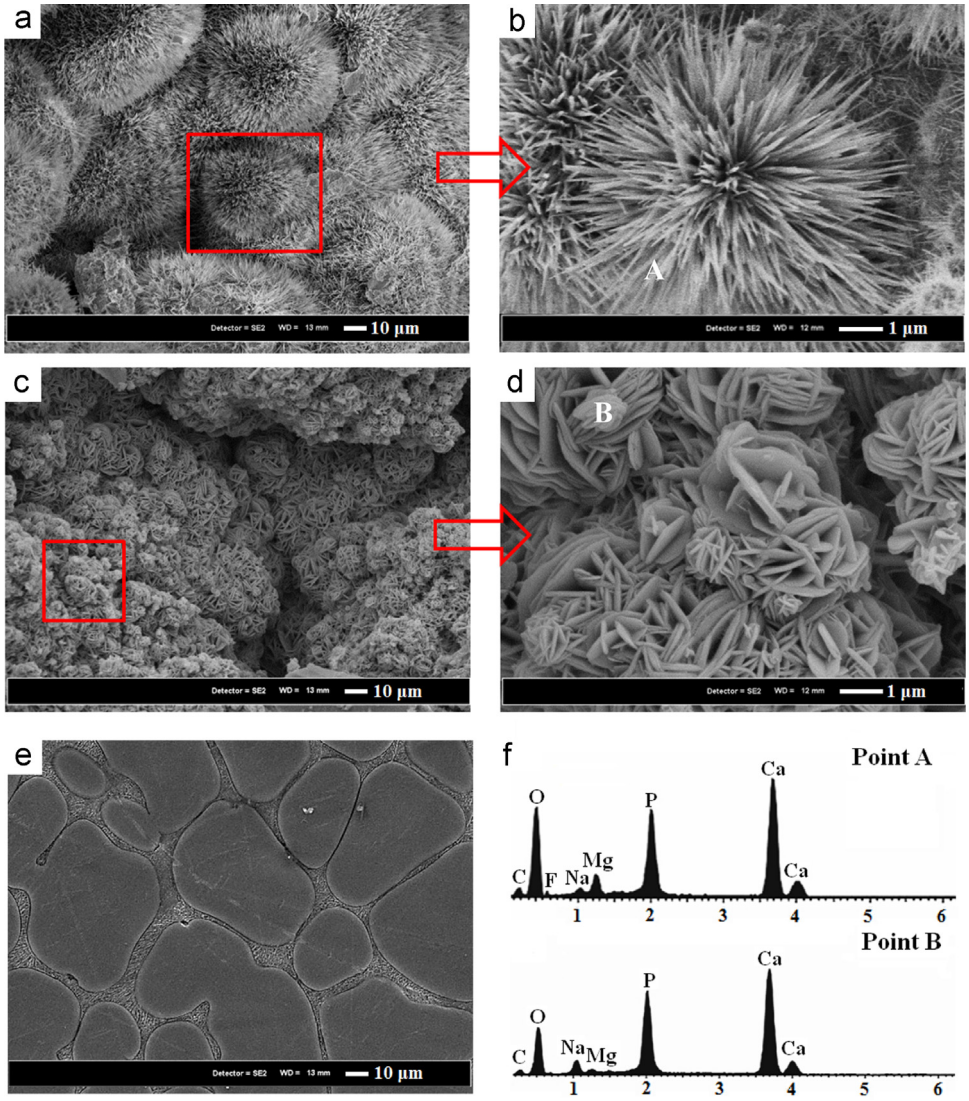

Fig. 1. SEM images of the surface of (a and b) FHA coated; (c and d) DCPD coated; (e) uncoated specimen and (f) EDS analysis of point A and point B.

diffraction angle. Fourier-transformed infrared (FTIR) spectroscopy was used to determine the surface functional groups of the calcium phosphate coating. The FTIR spectrum was recorded in a spectral range of 4000–450 cm^{-1}. Microstructural observation was performed by using a scanning electron microscope (JEOL JSM-6380LA), equipped with an EDS. Coating thickness was estimated by cross sectional FE-SEM observation of the FHA and DCPD coated specimens. A transmission electron microscope (Hitachi) was used to determine the size and morphology of the fine powders.

Rectangular specimens, with a surface area of 1 cm^2, were mounted in epoxy resin for electrochemical tests. The test was conducted at 37 °C in an open air glass cell containing 350 ml Kokubo solution with a pH of 7.66, using PARSTAT 2263 potentiostat/galvanostat (Princeton Applied Research). A three-electrode cell was used for potentiodynamic polarization tests. The reference electrode was saturated calomel electrode (SCE), the counter electrode was made of graphite rod, and the specimen was the working electrode. All experiments were carried out at a constant scan rate of 0.5 mV/s, initiated at −250 mV below the open-circuit potential.

For compression test, cylindrical specimens with a diameter of 10 mm and a height of 20 mm were immersed in SBF for 10 days, and then cleaned in a boiling solution of chromium trioxide (CrO_3) to remove the surface corrosion product. The specimens were then dried in warm air. Compression tests were performed using an Instron-5569 universal testing machine at a displacement rate of 1.0 mm/min, at ambient temperature. For each testing material, two specimens were examined.

The immersion tests of the uncoated, and DCPD, and FHA coated specimens were conducted according to the ASTM G31-72 standard. The specimens were washed thoroughly with distilled water, rinsed, ultrasonically degreased with ethanol, and subsequently dried at room temperature. The specimens were then immersed in a beaker containing 200 ml of Kokubo simulated body fluid (SBF). The average pH value of the SBF from three measurements was recorded during the soaking

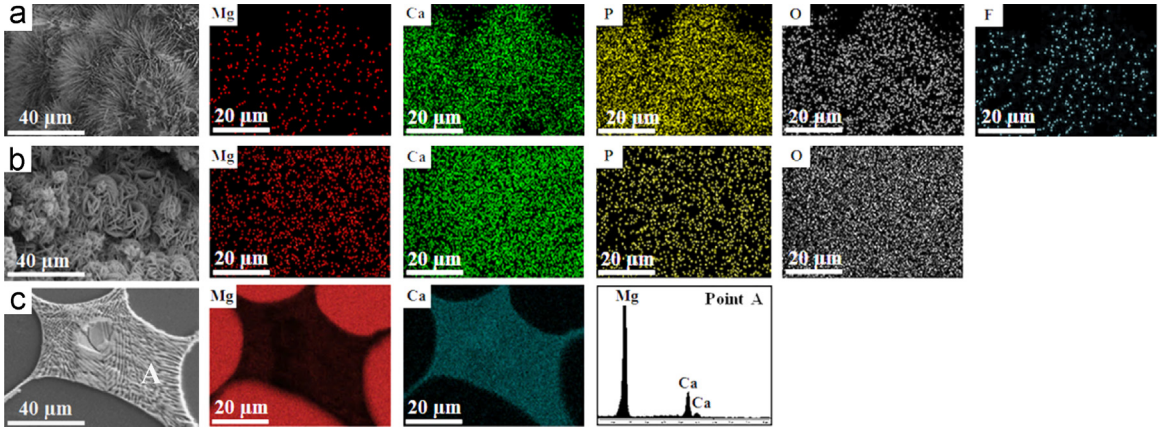

Fig. 2. SEM images and element mapping and corresponding EDS analysis of (a) FHA coated; (b) DCPD coated and (c) uncoated alloy (Mg→red; Ca→green; P→yellow; O→gray; and F→blue). (For interpretation of the references to color in this figure legend, the reader is referred to the web version of this article.)

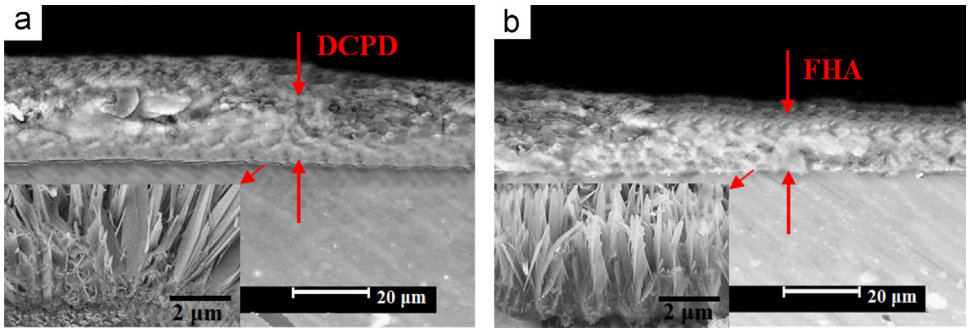

Fig. 3. Cross-sectional SEM image of (a) DCPD coated and (b) FHA coated specimen.

experiment after every 12 h interval. After the immersion test, the surface appearance of the corroded specimens was assessed using SEM and EDS. The hydrogen evolution rate of the specimens was also measured during the 240 h immersion in Kokubo solution experiment. Two replicas were immersed in a beaker while a funnel was located over the samples to collect evolved hydrogen in a buret above the funnel. The hydrogen evolution rate was calculated in ml/cm^2/day before renewing the solution.

3. Results and discussion

3.1. Microstructure and composition

Fig. 1 shows SEM images of the uncoated and DCPD, and FHA coated specimens. Fig. 1a and b shows that the FHA coating had dandelion-like aggregates of needle-shape crystals, covering the entire surface of the Mg alloy densely and uniformly without apparent defects. The main reason for heterogeneous nuclei formation on the surface is the use of a moderate current density which induces a super-saturation status in the vicinity of the substrate surface. Thus, providing an appropriate environment for dense and uniform structure formation [28]. The results of the EDS analysis showed that the coating was rich in calcium, phosphorus and oxygen (Fig. 1f). The atomic ratio of Ca/P of the coatings was about 1.38. Fig. 1c and d shows that the brushite coating had a flake-like structure, accompanied with some defects. The EDS analyses of DCPD coated specimens indicated that the coating layers consisted of magnesium, calcium, oxygen, carbon, and phosphorus, with Ca/P atomic ratio of 1.35 (Fig. 1f). The brushite is thermodynamically unstable and relatively soluble under physiological conditions. Thus, it is typically used as a precursor material for generating HA [29]. The microstructure of binary Mg–Ca consisted of α-Mg and Mg_2Ca secondary phases. The secondary phases are formed in the form of eutectic phases (α-Mg + Mg_2Ca) along the grain boundary (Fig. 1e). The corresponding EDS analysis in the mapping suggests that the denoted area, which is composed of Mg and Ca, is related to the evolution of Mg_2Ca phase.

Fig. 2 shows the mapping of the elements on the surface of uncoated, and DCPD, and FHA coated samples. The DCPD coating was predominantly composed of Ca, P, Mg and O while additional element, F, was detected in the FHA coating (Fig. 2a). It can be seen that all the elements were distributed homogeneously, indicating the formation of compact protective film on the substrate. The mapping of DCPD also shows similar elemental distribution on the substrate (Fig. 2b). However, elemental mapping of the uncoated sample showed high concentration of Ca at the grain boundaries (Fig. 2c).

Fig. 3a shows cross-sectional SEM image of the DCPD coated specimen, indicating dense coating with relatively

uniform thickness (16–20 μm). However, there are some micropores and microflaws in the film, but they are not entirely transverse in the coating. The thickness of the FHA coating is around 12–15 μm and there is a sound adhesion between the deposited coating and the underlying substrate (Fig. 3b). This indicates that the coating can be tightly adhered to the substrate.

The XRD patterns of Mg–Ca alloy shows the existence of relatively small, although discernible, peaks of Mg_2Ca phases with intensities of (110), (103), (112) and (313), accompanied by Mg peaks (Fig. 4a). Mg_2Ca has a hexagonal crystal structure with the space group P_{63}/mmc and the lattice parameters are $a=0.623$ nm and $c=1.012$ nm. The structure is similar to Mg but with almost twice the size of the unit cell [30]. The new peaks at $2\theta=21.1°$, 29.3°and 50.3° in the patterns correspond to dicalcium phosphate dihydrate (DCPD, brushite, $CaHPO_4 \cdot 2H_2O$) formed by ED [31]. The XRD results revealed that crystalline DCPD formed on the substrate surface accompanied with HA, no other calcium phosphate phases and $Mg(OH)_2$ were detected on the sample surface (Fig. 4b). The structures of DCPD has either a non-centrosymmetric, monoclinic space group I_a(C4s) with $Z=4$, or a centrosymmetric space group $I_{a/2}$ with unit cell parameters $a=0.5812$ nm, $b=1.5180$ nm, and $c=0.6239$ nm [32]. Magnesium peaks were also observed because the DCPD coating was not thick enough. FHA coated specimens indicated that the typical diffraction peaks at $2\theta=25.81°$, 31.6°, 32.1°, 32.7°, 34° and 36.8° were accompanied by small positional shifts towards higher angles, which is due to substitution of the F^- ion (1.32 Å) for the OH^- group (1.68 Å) during ED process (Fig. 4c). FHA also has a very similar atomic structure and belongs to the same space group as HA (space group: $P6_3/m$; parameters: $a=b=9.462$ Å and $c=6.849$ Å, $\alpha=\beta=90°$, $\gamma=120°$). The replacement of OH^- ion by F^- leads to a contraction in the a-axis to 0.9368 nm; however, no significant change was observed in the c-axis. The substitution of F^- ion for OH^- ion in the host HA crystals does not signifiantly affect the morphology of the HA particles [17]. FHA showed higher thermal stability than HA due to the replacement of OH^- groups in the fluorapatite structure by F^- ion [22]. The average crystallite size of the DCPD, and FHA coated samples was determined by Scherrer's method. In this method, the (021) and (211) peaks were considered as the most obvious peaks for calculating the average particle size of the DCPD and FHA coated samples, respectively. The calculated crystallite size of the DCPD and FHA coated specimens was 210 nm and 72 nm, respectively. Fig. 5 shows the TEM image and related selected area diffraction patterns (SADP) of the DCPD and

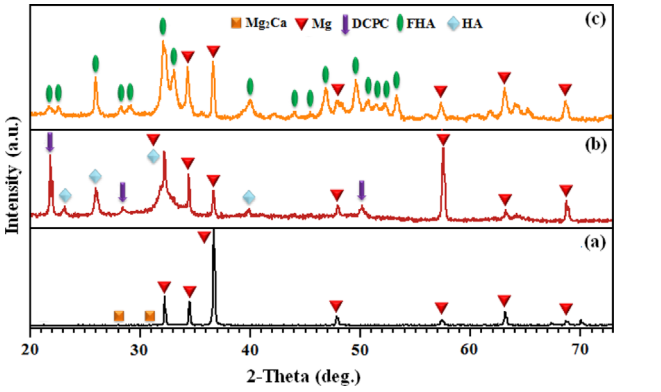

Fig. 4. X-ray diffraction patterns of (a) uncoated Mg alloy; (b) DCPD coated; and (c) FHA coated specimen.

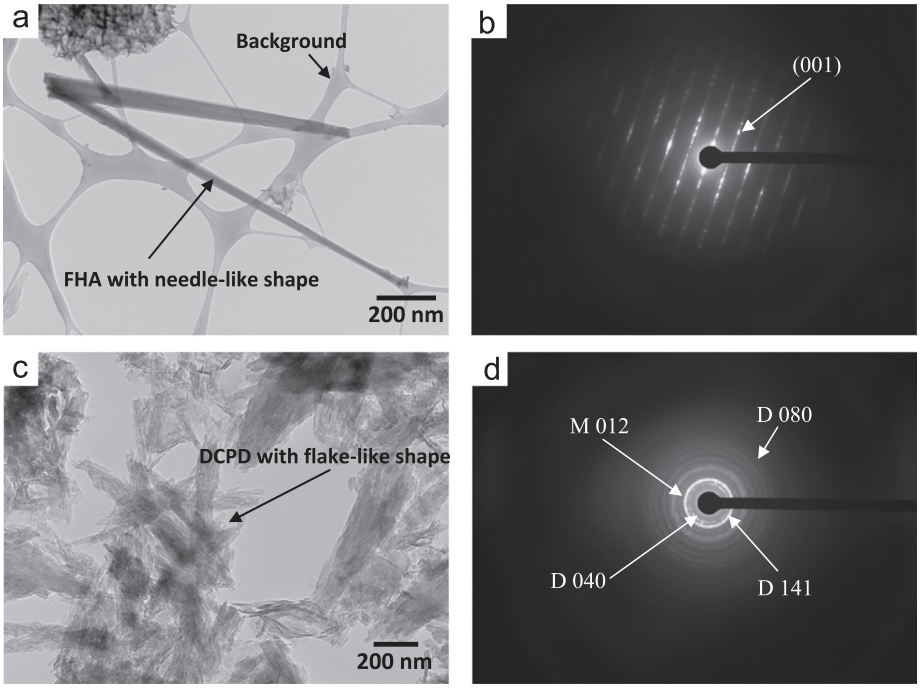

Fig. 5. TEM micrographs with selected-area diffraction pattern of (a) FHA coated; (b) SADP of FHA coated; (c) DCPD coated specimen; and (d) SADP of DCPD coated.

FHA coatings. It was found that the needle-like particles formed in the FHA coatings are about 72–90 nm in diameter and 2–2.5 μm in length (Fig. 5a). The clear SADP of the tip of the needle-like crystal showed that well-crystallized FHA was formed and the long axis of the needle was along [001] axis of FHA, indicating that the needle-like FHA crystals grew along [001] axis (Fig. 5b). The DCPD crystal has a lath-like shape with 150–250 nm width and 700 nm–1 μm length. The diffraction of DCPD nanosized crystallites shows a continuous ring patterns with no d-spacing of HA (Fig. 5d).

The mechanism of electrolytic deposition can be described as a series of electrochemical reactions. The three possible sources of OH^- at the cathode are [27,33]:

$$O_2 + 2H_2O + 4e^- \rightarrow 4OH^- \quad (2)$$

$$NO_3^- + H_2O + 2e^- \rightarrow 2OH^- + NO_2^- \quad (3)$$

$$2H_2O + 2e^- \rightarrow H_2 + 2OH^- \quad (4)$$

Hydroxide ions, generated during the electrodeposition process, resulted in an increase of the pH in the vicinity of the cathode; which led to the occurrence of the following reactions:

$$H_2PO_4^- + e^- \rightarrow HPO_4^{2-} + 1/2H_2 \quad (5)$$

$$H_2PO_4^- + 2e^- \rightarrow PO_4^{3-} + H_2 \quad (6)$$

$$H_2PO_4^- \rightarrow HPO_4^{2-} + H^+ \quad (7)$$

$$HPO_4^{2-} \rightarrow PO_4^{3-} + H^+ \quad (8)$$

The precipitation of phosphate ions occurred due to the acid–base reactions, which are vital for the crystallization process of formation of FHA coating film according to the following reaction:

$$H_2PO_4^- + OH^- \rightarrow HPO_4^{2-} + H_2O \quad (9)$$

$$H_2PO_4^- + H_2O + 2e^- \rightarrow H_2PO_3^- + 2OH^- \quad (10)$$

The suitable local chemical environment in the vicinity of the cathode enabled the HPO_4^{2-} ions to react with the Ca^{2+} ions, producing the DCPD which precipitated on the surface of the substrate through the following reaction [21,34]:

$$Ca^{2+} + HPO_4^{2-} + H_2O \rightarrow CaHPO_4 \cdot 2H_2O \quad (11)$$

The DCPD coating, after alkaline treatment, was converted to HA according to the following reaction:

$$10CaHPO_4 + 2OH^- \rightarrow Ca_{10}(PO_4)_6(OH)_2 + 4PO_4^{3-} + 10H^+ \quad (12)$$

Calcium deficient hydroxyapatite (CDHA) was formed as follows [35]:

$$(10-x)Ca^{2+} + (6-x)PO_4^{3-} + xHPO_4^{3-} + xHPO_4^- + (2-x)OH^- \rightarrow Ca_{10-x}(HPO_4)_x(PO_4)_{6-x}(OH)_{2-x}$$
where $0 < x \leq 2$. (13)

Addition of NaF into the electrolyte led to the occurrence of the following reactions. At the early stage, Ca^{2+} ions rapidly consumed the F^- ions in the electrolyte to form CaF_2 which can be expressed as follows [21]:

$$Ca_5(PO_4)_3OH + 10F^- + (7-n)H^+ \rightarrow 5CaF_2 + H_2O + (3-n)H_2PO_4^- + nH_2PO_4^{2-} \quad (14)$$

Afterwards, CaF_2 particles reacted with the HPO_4^{2-} ions in the solution to form FHA [21]:

$$5CaF_2 + (3-n)H_2PO_4^- + nH_2PO_4^{2-} + (1-x)H_2O \rightarrow Ca_5(PO_4)_3(OH)_{1-x}F_x + (10-x)F^- + (7-x-n)H^-$$
$(0 < x < 1,\ 0 < n < 3)$ (15)

Combining reactions (14) and (15), resulted in the formation of FHA via the following reaction:

$$10Ca^{2+} + 6PO_4^{3-} + xF^- + (2-x)OH^- \rightarrow Ca_{10}(PO_4)_6F_x(OH)_{2-x} \quad (16)$$

The bonding of F–H with adjacent OH^- along the *c*-axis can occur as the F^- ions are doped; the orientation of O–H in FHA crystals is then increased and vertical FHA crystals are produced. This finding is in good agreement with XRD and FTIR results.

3.2. Mechanical properties

Table 1 shows the compression strength of the uncoated Mg–Ca, and DCPD, and FHA coated specimens before and after immersion in SBF for duration of 10 days. The compression strength of the uncoated Mg–Ca sample before immersion was 242.7 MPa and this value decreased to 159.2 MPa after immersion in SBF. However, the compression strength of the DCPD and FHA coated samples was 182.4 MPa and 203.6 MPa after immersion, respectively. These values are comparable to the compressive strength of human bones (100–230 MPa) in cortical bone. Apparently, the compression strength of the FHA coated sample after immersion is 22% higher compared to the uncoated sample (Fig. 6). These results showed that Ca–P coating can delay the loss of the mechanical property of Mg–Ca alloy. Due to the protection of the coating film, the compressive load of the samples with Ca–P coating after immersion for 10 days is much higher than that of uncoated sample. However, the DCPD coated sample shows higher degradation rates compared to FHA coated sample due to higher solubility of DCPD in the SBF. The FHA coated sample showed the highest compressive strength after immersion. This is attributed to larger specific surface area of the nanophase of the FHA coating, which provided more sites for the absorption of Ca^{2+}, Mg^{2+} and PO_4^{3-} from SBF, hence, providing better protection. Therefore, it may be deduced that the FHA coating is more chemically stable in SBF compared to the DCPD coating, as a result of their higher crystallinity and denser lattice structure; resulted in higher protection for the substrate, acting as a barrier against ion diffusion [36]. Therefore, the coating can effectively postpone the decline of compressive properties of the uncoated sample, and provide sufficient support for the post-fracture bone healing.

Table 1
Compression test results of the uncoated Mg–Ca, DCPD and FHA coated alloys before and after immersion in SBF.

Specimen	Uncoated Mg–3Ca alloy before immersion	FHA coated alloy after 10 days immersion	DCPD coated alloy after 10 days immersion	Uncoated Mg–Ca alloy after 10 days immersion
Compression strength – UCS (MPa)	242.7	203.6	182.4	159.2

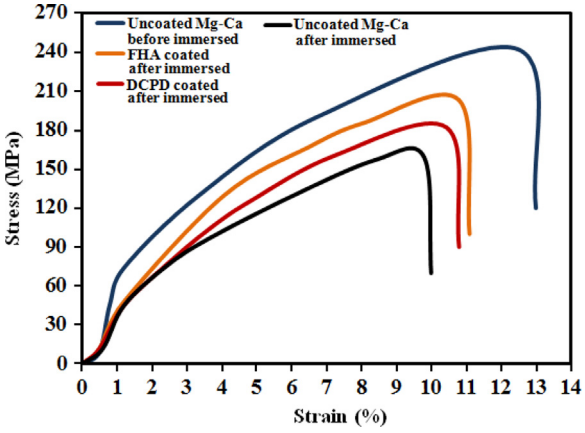

Fig. 6. Compressive stress–strain curves for uncoated, DCPD and FHA coated specimens before and after immersion in SBF.

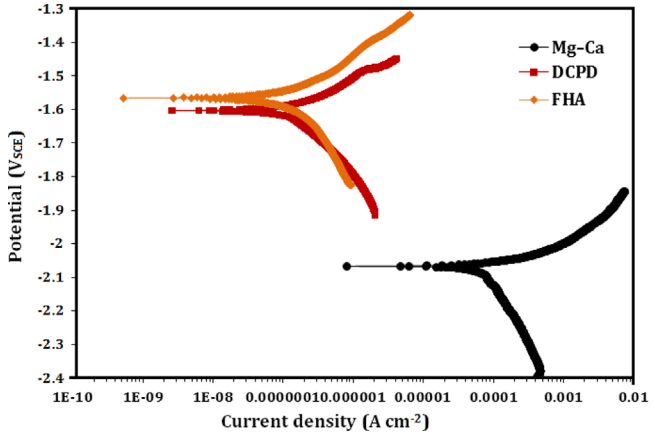

Fig. 7. Potentiodynamic polarization curves of uncoated alloys, DCPD and FHA coated specimens in Kokubo solution.

3.3. Electrochemical measurement

Fig. 7 shows cathodic and anodic polarization curves of the DCPD, and FHA coated and uncoated specimens in the Kokubo solution. The corrosion potential of uncoated Mg–Ca, and DCPD, and FHA coated specimens is −2066.8 mVSCE, −1602.7 mVSCE and −1565.7 mVSCE respectively. This shift means that the corrosion reaction of Mg–Ca alloy is suppressed by the Ca–P coating. It is suggested that the densely packed needle-like precipitates can prevent the solution from penetrating into the substrate. This barrier effect is enhanced with the growth of the needle-like precipitates to be the inner dense layer. The anodic polarization curves of the uncoated specimen shows a breakdown immediately after the initiation of polarization. The corrosion current density (i_{corr}) of the uncoated, and DCPD, and FHA coated specimens is 314.2, 6.12 and 5.52 μA/cm^2 respectively. The lower i_{corr} value of Ca–P coated sample indicates a lower degradation rate. This result indicates that the protectiveness of the FHA coating is higher than that of the DCPD coating. This higher protectiveness is due to the enhancement of the barrier effect of the inner layer against the solution penetration. The corrosion current density (i_{corr}), corrosion potential (E_{corr}), cathodic Tafel slopes (β_c), anodic Tafel slopes (β_a) and the corresponding corrosion rate (P_i) of specimens extracted from the polarization curves are shown in Table 2. The i_{corr} is related to the corrosion rate (P_i) according to following equation [37,38]:

$$P_i = 22.85 i_{corr} \tag{17}$$

According to Eq. (17), the corrosion rate of the uncoated Mg–Ca alloy was 7.17 mm/year. However, FHA (0.13 mm/year) and DCPD (0.14 mm/year) coated specimens showed lower corrosion rate compared to the uncoated alloy. The linear polarization resistance, R_p, which is inversely proportional to the value of the corrosion current density, is calculated according to the following equation [39]:

$$R_p = \frac{\beta_a \beta_c}{2.3(\beta_a + \beta_c) i_{corr}} \tag{18}$$

The polarization resistance of FHA and DCPD is 4.61 and 3.31 kΩ cm^2, respectively. These values are significantly higher than that of the uncoated alloy (0.095 kΩ cm^2). It can be seen that the corrosion resistance of the Mg alloy significantly improved, after Ca–P coating. The enhancement of the R_p value after coating is related to the formation of barrier Ca–P film on the substrate, which inhibits the corrosive SBF from penetrating into the substrate. The higher corrosion resistance of the FHA coating, compared to the DCPD coating, is due to formation of more uniform and compact protective film; which can provide better protection for the substrates. This compact barrier film at the interface of the substrate and the FHA layer can effectively reduce diffusion of the corrosive medium into the substrate and hence, decline the corrosion rate. The difference between chemical composition of FHA, and DCPD coating is another reason for higher corrosion rate of DCPD, compared to FHA. This can explain why the latter is more stable in SBF solution than DCPD.

Table 2
Electrochemical parameters of uncoated, DCPD and FHA coated alloy in Kokubo solution attained from the polarization test.

Alloy	Corrosion potential, E_{corr} (mV vs. SCE)	Current density, i_{corr} (μA/cm^2)	Cathodic slope, β_C (mV/decade) vs. SCE	Anodic slope, β_a (mV/decade) vs. SCE	Polarization resistance, R_p (kΩ cm^2)	Corrosion rate, P_i (mm/year)
Mg–3Ca alloy	−2066.8	314.2	247	96	0.095	7.17
DCPD coated	−1602.7	6.12	342	54	3.31	0.14
FHA coated	−1565.7	5.52	387	69	4.61	0.13

3.4. Immersion test

The pH variation in the Kokubo solution with samples immersed for 240 h is shown in Fig. 8. The pH monitoring method has been used in several researches where lower pH value represented lower corrosion rate of the alloy [34,40]. It can be seen that the pH values of the Kokubo solution with immersed DCPD, and FHA coated alloys are clearly lower than that of the uncoated sample over the time range. It is also observed that the pH values of the Kokubo solution increase in the order of FHA < DCPD < uncoated samples. It is obvious that presence of fluorine ion in the coating layer caused a reduction in pH during immersion in the SBF [23]. For all the samples, the degradation of $Mg(OH)_2$ contributed most to the rapid increase in the initial pH due to the release of OH^- ions [19]. However, the pH value became stabilized over longer immersion times. This may be due to the penetration of the solution into the interface between Ca–P coating and substrate via the pores and cracks of the coating when corroded by the SBF. The precipitation of apatite, which consumed OH^- ions, could be another reason for the minimal pH increase at the final stage [41]. In this regard, the real surface-fluid contact area is larger for the FHA coating. Thus, there would be more apatite precipitate from the solution on the coating within the same amount of time, which leads to decreasing the pH values of the solution.

Fig. 9 shows the surface morphology of the uncoated, and DCPD, and FHA coated samples after being immersed in SBF for 240 h. Corrosion products cover some part of uncoated alloy surface. Deep cracks also formed due to dehydration of the surface layer in the air (Fig. 9a and b). DCPD coating presented flake-like structure covered the entire alloy surface (Fig. 9c and d). However, the DCPD has more porosity than FHA coating, making it more prone to dissolving in SBF. Furthermore, due to the inhomogeneous structure of the DCPD, the rate of degradation was not the same over different areas. Therefore, it does not provide satisfactory corrosion resistance for long-term and it does not sufficiently meet the required criteria for bone healing. The EDS analysis of the corrosion product of the DCPD coating revealed the presence of Na, Mg, Ca, P, and O. The Ca/P molar ratio of the compound is 1.39 (Fig. 9f). Coarse needle-like crystals of FHA observed on the sample surface which their crystals grew in size and increased in number by increasing immersion time (Fig. 9e). Formation of needle-like crystals may be due to the

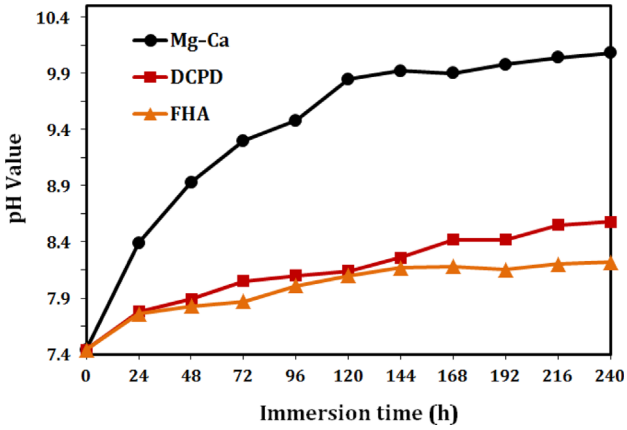

Fig. 8. Change in pH of the Kokubo solution during immersion of uncoated Mg alloy, DCPD and FHA coated specimens for duration of 240 h.

clustering and grain growth along *c*-axis from this primary swirl-like layer [42]. The EDS analysis of the corrosion product of FHA coating revealed the presence of F, Mg, Ca, P, and O. The Ca/P molar ratio of the compound was 1.47 (Fig. 9f). Based on Kim′s theory [43], in the early stage of apatite formation after the sample is immersed in the SBF, the HA particles possess negative surface charge. This can be attributed to the presence of hydroxyl and phosphate groups. Hence, the negative ions of OH^- and HPO_4^{2-} interact with the positive Ca^{2+} ions to form the Ca-rich amorphous calcium phosphate (ACP) for enabling positive surface charge within the immersing sample in the SBF. Then, the formed Ca-rich ACP on the surface of HA interacts with the negative phosphate ion in the SBF to form Ca-poor ACP, which eventually crystallizes into bone-like apatite. Based on the aforementioned mechanism, due to the replacement of OH^- by F^- in the surface layer of the apatite, the negative surface charge of the apatite in the SBF rises considerably. This resulted in more Ca^{2+} ions being attracted in the Ca-rich ACP due to the smaller ion radii and stronger electronegativity of F^- compared to OH^-. Hence, the nucleation of bone-like apatite is significantly enhanced in the surface layer of FHA coated sample; which can accelerate bone healing process [23].

Fig. 10 shows a schematic illustration of corrosion mechanism of Ca–P coated Mg–Ca alloy. When Ca–P coated specimens are immersed in the SBF, the MgO in the outer layer starts to react with the corrosive solution and converts to $Mg(OH)_2$ (Fig. 10b). The amount of this corrosion product is less

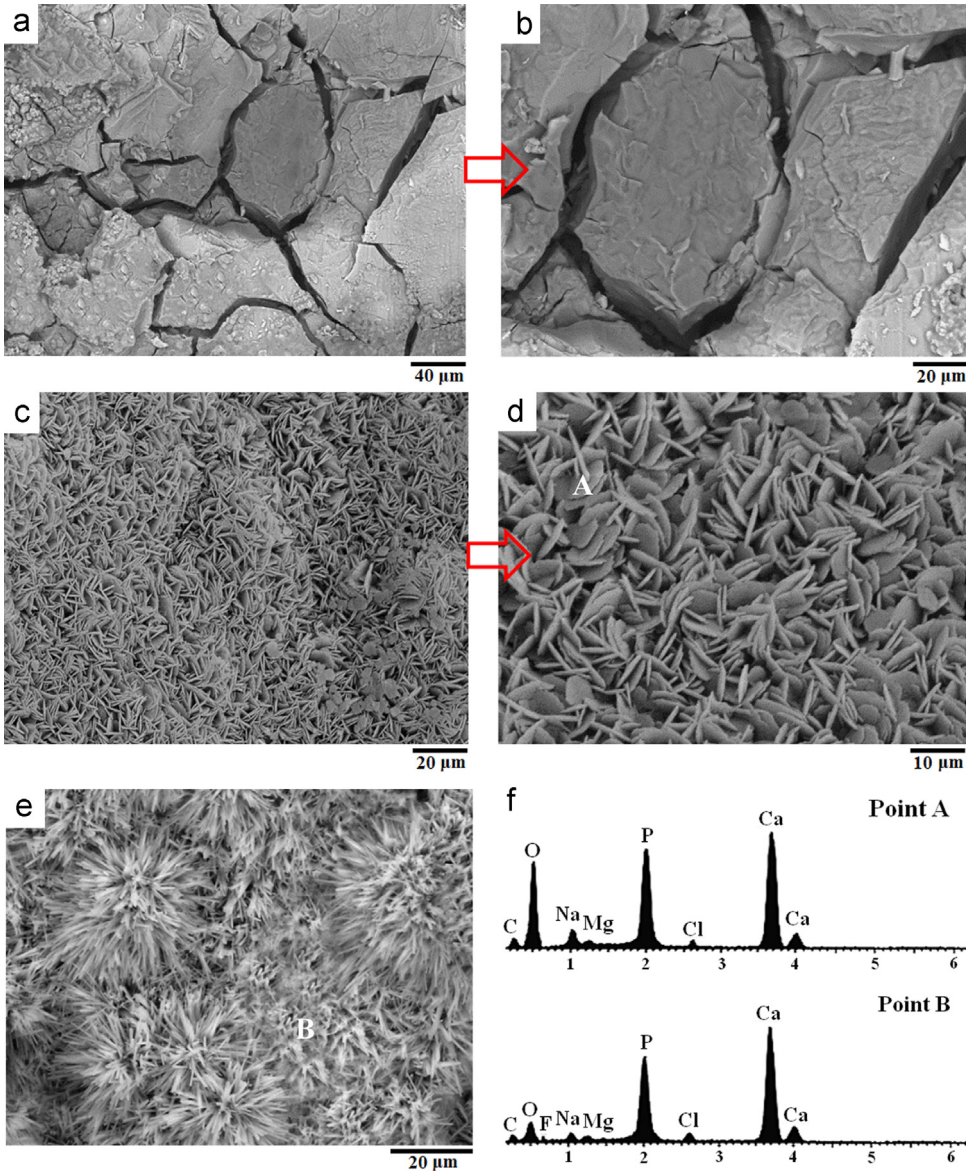

Fig. 9. SEM images of (a and b) uncoated Mg alloy; (c and d) DCPD coated; (e) FHA coated samples after immersion into Kokubo for 240 h duration and (f) EDS analysis of point A and point B.

significant at the early stage of immersion, owing to the lower amount of MgO compared to the Mg in the substrate. Formation of $Mg(OH)_2$ resulted in reaction with other constituents in the SBF and the local alkalization leads to the formation of a number of precipitates [40]. The hydroxyapatite is formed on the Ca–P coatings layer due to the dissolution of high amounts of Mg^{2+} and reaction of phosphate ions (HPO_4^{2-} or PO_4^{3-}) and Ca^{2+} in the solution with OH^- ions to form HA (Fig. 10c). Finally, the amount of precipitates increased on the coating layer with increasing immersion time and some of the corrosion products are left on the coating layer; which reduces the degradation rate of the substrate (Fig. 10d). The XRD pattern confirmed the presence of $Mg(OH)_2$ as main corrosion product of the uncoated and DCPD coated alloys (Fig. 11). However, the XRD pattern of FHA coated specimens showed the presence of only FHA and Mg even after 240 h of exposure to SBF. The resulting precipitated Ca–P on the surface of the coated alloy reduces the penetration rate of the solution via the coating layer defects. Therefore, the corrosion rate of the substrate declined as a result of high thermodynamic and structural stability of Ca–P and its barrier action between the SBF and coating layer defects. XRD indicated higher intensities of the DCPD phase with lower intensities of $Mg(OH)_2$ phases from the Ca–P coated alloy, compared to the uncoated alloy. This implies that a lesser amount of $Mg(OH)_2$ corrosion product was formed on the surface of DCPD coated alloy, an acceptable result as it has a lower corrosion rate than that of the uncoated alloy. In comparison, the FHA coating with more dense and uniform layer before immersion, acts as an effective protective layer to prevent further corrosion attack. It can be seen that no significant presence of $Mg(OH)_2$ was detected in the corrosion

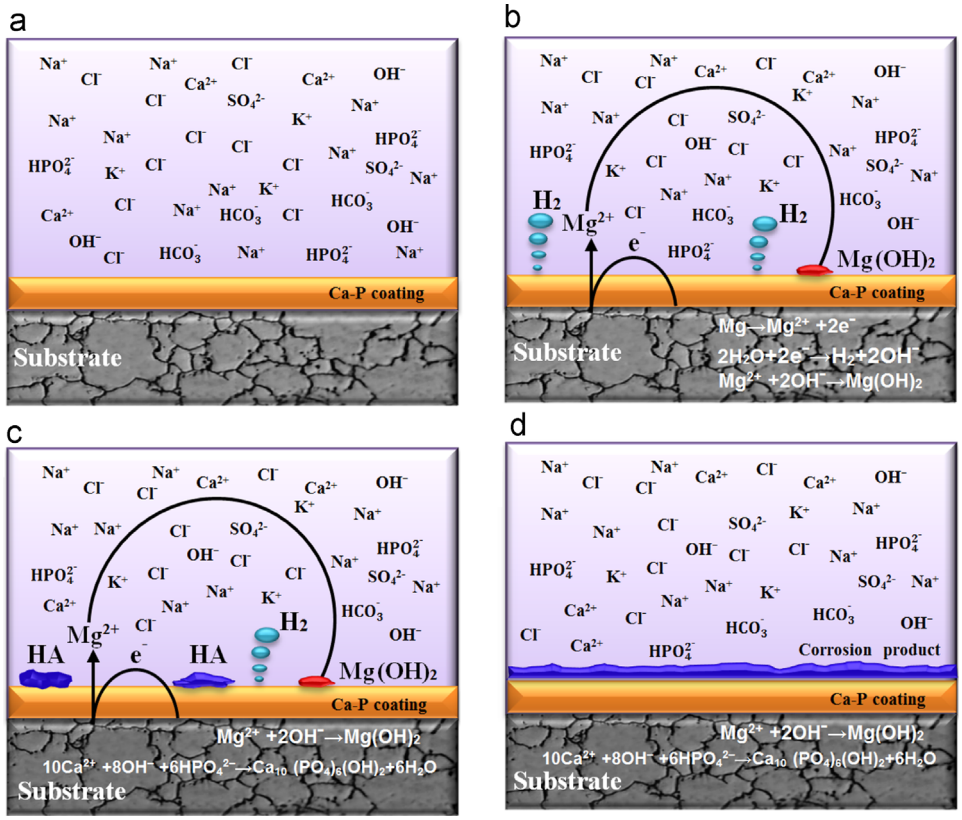

Fig. 10. Schematic illustration of the degradation process of the Ca–P coating upon long term corrosion in SBF.

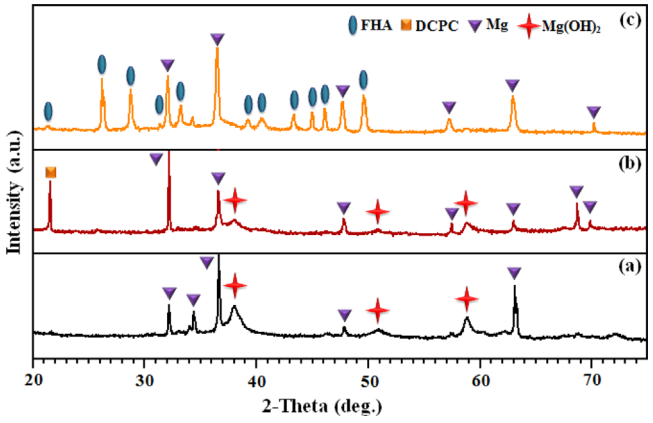

Fig. 11. X-ray diffraction patterns attained from the corrosion products of (a) uncoated alloy; (b) DCPD coated; and (c) FHA coated specimen after full immersion exposure to SBF solution for 240 h duration.

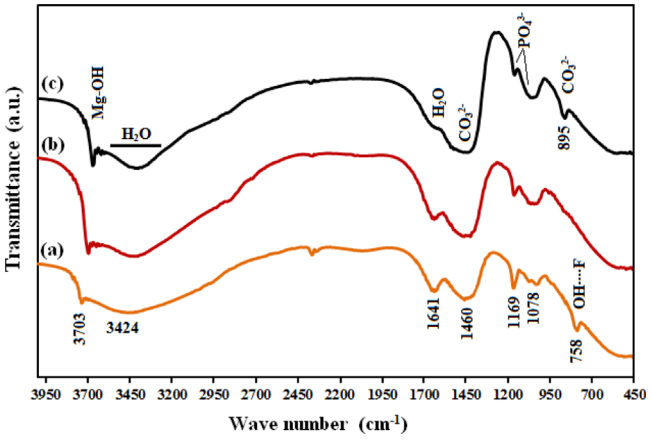

Fig. 12. FTIR absorption spectra obtained from the corrosion products of (a) FHA coated; (b) DCPD coated and (c) uncoated alloy; after immersion exposure to SBF solution for 240 h duration.

products obtained from FHA coating, indicating that less corrosion attack occurred in the case of FHA coated samples.

The FTIR analysis of the corrosion products of coated and uncoated specimens are shown in Fig. 12. The coated and uncoated specimens gave a peak at 3703 cm^{-1}, corresponding to $Mg(OH)_2$ as the main corrosion product. This phase is more visible for untreated, and DCPD coated specimens, compared to the FHA coated specimens. The broad absorption band at 3424 cm^{-1} is due to the vibration of water molecules. The band at 1641 cm^{-1} is also attributed to the presence of water in the samples. Formation of apatite is further confirmed by FTIR in all surface specimens after immersing in SBF, proving the formation of white bone-like apatite particles. The P−O stretching of phosphate groups (1169 and 1078 cm^{-1}) was observed after immersing specimens in SBF for 10 days. It was reported that phosphate ions HPO_4^{2-} can capture OH^- ions which are produced via the cathodic reaction and decline massive precipitation of $Mg(OH)_2$ [44]. The C−O stretching of carbonate groups at 1460 cm^{-1} and 895 cm^{-1} is also observed, indicating the formation of hydroxyapatite. The appearance of OH…F stretching band at 758 cm^{-1} is indicative of

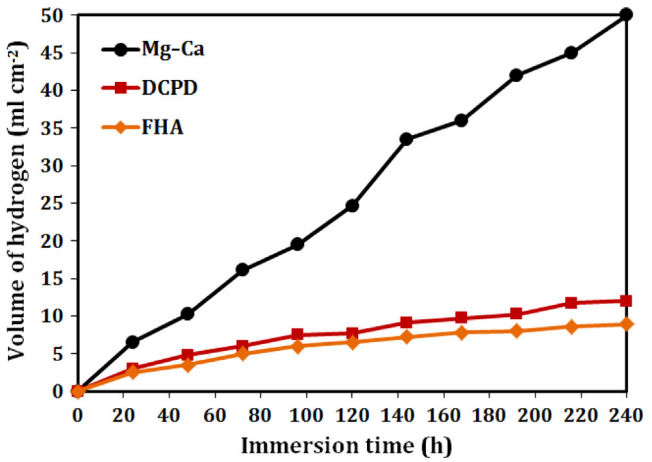

Fig. 13. Hydrogen evolution of the uncoated Mg alloy, DCPD and FHA coated specimens immersed in Kokubo solution for duration of 240 h.

the substitution of the F^- ions for OH^- ions [44]. The precipitation of HA on the surface of the specimens can accelerate healing of the bone tissue, indicating good biocompatibility of the alloy. The hydrogen evolution results of the coated and uncoated specimens in the Kokubo solution, for a period of 240 h, are shown in Fig. 13. The hydrogen evolution rate of the FHA, and DCPD coated specimen is 0.92 ml/cm^2/day and 1.23 ml/cm^2/day, respectively. These values are lower than the hydrogen desorption rate that could be tolerated by the human body (2.25 ml/cm^2/day) [45]. However, uncoated Mg–Ca alloys showed the highest hydrogen evolution rate (4.98 ml/cm^2/day). The rapid evolution of hydrogen bubbles resulted in significant subcutaneous gas pockets, which may delay the healing of surgical region, result in necrosis of tissues and cause discomfort [45]. The rate of degradation decreased in coated samples since Ca–P coating considerably hinder the degradation of the alloy. The degradation rate of the FHA was much slower than that of the uncoated sample. Thus it can be concluded that the FHA, with doped F^- ions, is more chemically stable in the SBF compared to the DCPD coating, owing to their higher crystallinity and denser lattice structure [46]. The decline in degradation rate of FHA can be also explained by the accumulation of the corrosion products which formed a protective layer on the surface of the coated alloy, retarding the corrosion process. However, both the hydrogen evolution rates of FHA and DCPD are significantly lower than the tolerance level in the human body which indicates higher corrosion resistance of Ca–P coated specimen compared to untreated one, in terms of corrosion current, hydrogen evolution rate and corrosion product content.

4. Conclusions

In this study, both nano-FHA, and DCPD coatings were deposited on the Mg–Ca alloy by ED method. The FHA coating had nanoneedle-like microstructure with crystallite size of around 72–90 nm while DCPD coating showed cauliflower shape microstructure with larger crystallite size (150–250 nm). The compression tests showed that the loss of the compressive integrities of the Mg alloy can be postponed by FHA and DCPD coatings. The potentiodynamic polarization indicated that the FHA, and DCPD coated samples have lower corrosion current density and higher polarization resistance, compared to the uncoated Mg alloy. Also, the FHA coated sample demonstrated lower degradation rate and higher corrosion resistance than the DCPD coated and uncoated samples. A model for corrosion mechanism of Ca–P coated magnesium alloy in the SBF is proposed. It is found that corrosion product layer on the surface of Ca–P coating during corrosion process can significantly inhibit Mg–Ca alloy from degrading. The nano-FHA coating was more dense and uniform with slower degradation rate and better apatite-inducing ability, suggesting that they can be promising for biodegradable medical applications.

Acknowledgments

The authors would like to acknowledge the Ministry of Higher Education of Malaysia and Universiti Teknologi Malaysia (UTM) for providing research facilities and financial support. The authors also thank Mr. Bolarinwa Komolafe for reading and improving the quality of language of the paper.

References

[1] H. Tang, D. Yu, Y. Luo, F. Wang, Preparation and characterization of HA microflowers coating on AZ31 magnesium alloy by micro-arc oxidation and a solution treatment, Appl. Surf. Sci. 264 (2013) 816–822.
[2] G.L. Song, S.Z. Song, A possible biodegradable magnesium implant material, Adv. Eng. Mater. 94 (2007) 298–302.
[3] K.Y. Chiu, M.H. Wong, F.T. Cheng, H.C. Man, Characterization and corrosion studies of fluoride conversion coating on degradable Mg implants, Surf. Coat. Technol. 202 (2007) 590–598.
[4] M.P. Staiger, A.M. Pietak, J. Huadmai, G. Dias, Magnesium and its alloys as orthopedic biomaterials: a review, Biomaterials 27 (2006) 1728–1734.
[5] L. Xu, F. Pan, G. Yu, In vitro and in vivo evaluation of the surface bioactivity of a calcium phosphate coated magnesium alloy, Biomaterials 30 (2009) 1512–1523.
[6] C. Lorenz, G.J. Brunner, P. Kollmannsberger, Effect of surface pre-treatments on biocompatibility of magnesium, Acta Biomater. 5 (2009) 2783–2789.
[7] K. Oh-Ishia, R. Watanabeb, C.L. Mendisa, Age-hardening response of Mg–0.3 at% Ca alloys with different Zn contents, Mater. Sci. Eng. A 526 (2009) 177–184.
[8] Y. Lu, L. Tan, B. Zhang, J. Lin, K. Yang, Synthesis and characterization of Ca–Sr–P coating on pure magnesium for biomedical application, Ceram. Int. 08 (2013) 132.
[9] J. Jayaraj, C.L. Mendis, T. Ohkubo, Enhanced precipitation hardening of Mg–Ca alloy by Al addition, Scr. Mater. 63 (2010) 831–834.
[10] X. Wang, S. Cai, T. Liu, M. Ren, Fabrication and corrosion resistance of calcium phosphate glass-ceramic coated Mg alloy via a PEG assisted sol–gel method, Ceram. Int. ⟨http://dx.doi.org/10.1016/j.ceramint.2013.09.093⟩.
[11] A. Seyfoori, S. Mirdamadi, A. Khavandi, Z. Seyed Raufi, Biodegradation behavior of micro-arc oxidized AZ31 magnesium alloys formed in two different electrolytes, Appl. Surf. Sci. 261 (2012) 92–100.
[12] H.R. Bakhsheshi-Rad, M.H. Idris, M.R.A. Kadir, M. Daroonparvar, Effect of fluoride treatment on corrosion behavior of Mg−Ca binary alloy for implant application, Trans. Nonferr. Met. Soc. China 23 (2013) 699–710.

[13] Y. Huang, Y. Yan, X. Pang, Q. Ding, S. Han, Bioactivity and corrosion properties of gelatin-containing and strontium-doped calcium phosphate composite coating, Appl. Surf. Sci. 282 (2013) 583–589.
[14] J. Zhang, C.S. Dai, J. Wei, Z.H. Wen, Study on the bonding strength between calcium phosphate/chitosan composite coatings and a Mg alloy substrate, Appl. Surf. Sci. 261 (2012) 276–286.
[15] S.V. Dorozhkin, Calcium orthophosphates in nature, Biol. Med. Mater. 2 (2009) 399–498.
[16] S. Shadanbaz, G.J. Dias, Calcium phosphate coatings on magnesium alloys for biomedical applications: a review, Acta Biomater. 8 (2012) 20–30.
[17] Y. Chen, X. Miao, Effect of fluorine addition on the corrosion resistance of hydroxyapatite ceramics, Ceram. Int. 30 (2004) 1961–1965.
[18] H. Farnoush, A. Sadeghi, A.A. Bastami, A. Khavandi, et al., An innovative fabrication of nano-HA coatings on Ti–CaP nanocomposite layer using a combination of friction stir processing and electrophoretic deposition, Ceram. Int. 39 (2013) 1477–1483.
[19] E.C. Meng, S.K. Guan, H.X. Wang, L.G. Wang, Effect of electrodeposition modes on surface characteristics and corrosion properties of fluorine-doped hydroxyapatite coatings on Mg–Zn–Ca alloy, Appl. Surf. Sci. 257 (2011) 4811–4816.
[20] M. Kheradmandfard, M.H. Fathi, Fabrication and characterization of nanocrystalline Mg-substituted fluorapatite by high energy ball milling, Ceram. Int. 39 (2013) 1651–1658.
[21] J. Wang, Y. Chao, Q. Wan, Z. Zhu, H. Yu, Fluoridated hydroxyapatite coatings on titanium obtained by electrochemical deposition, Acta Biomater. 5 (2009) 1798–1807.
[22] M.H. Fathi, E.M. Zahrani, A. Zomorodian, Novel fluorapatite/niobium composite coating for metallic human body implants, Mater. Lett. 63 (2009) 1195–1198.
[23] M.H. Fathi, E.M. Zahrani, Mechanical alloying synthesis and bioactivity evaluation of nanocrystalline fluoridated hydroxyapatite, J. Cryst. Growth 311 (2009) 1392–1403.
[24] H.W. Kim, H.E. Kim, J.C. Knowles, Fluor-hydroxyapatite sol–gel coating on Ti substrate for hard tissue implants, Biomaterials 25 (2004) 3351–3358.
[25] E.A. Abdel-Aal, D. Dietrich, S. Steinhaeuser, B. Wielage, Electrocrystallization of nanocrystallite calcium phosphate coatings on titanium substrate at different current densities, Surf. Coat. Technol. 202 (2008) 5895–5900.
[26] Y.W. Song, D.Y. Shan, E.H. Han, Electrodeposition of hydroxyapatite coating on AZ91D magnesium alloy for biomaterial application, Mater. Lett. 62 (2008) 3276–3279.
[27] C. Wen, S. Guan, L. Peng, C. Ren, X. Wang, Z. Hu, Characterization and degradation behavior of AZ31 alloy surface modified by bone-like hydroxyapatite for implant applications, Appl. Surf. Sci., 255, , 2009, p. 6433–6438.
[28] R. Hu, C. Lin, H. Shi, H. Wang, Electrochemical deposition mechanism of calcium phosphate coating in dilute Ca–P electrolyte system, Mater. Chem. Phys. 115 (2009) 718–723.
[29] A. Yanovska, V. Kuznetsov, A. Stanislavov, S. Danilchenko, L. Sukhodub, Calcium–phosphate coatings obtained biomimetically on magnesium substrates under low magnetic field, Appl. Surf. Sci. 258 (2012) 8577–8584.
[30] N.T. Kirkland, N. Birbilis, J. Walker, In-vitro dissolution of magnesium–calcium binary alloys: clarifying the unique role of calcium additions in bioresorbable magnesium implant alloys, J. Biomed. Mater. Res. Part B: Appl. Biomater. 95B (2010) 91–100.
[31] S. Yang, Q. Min, C. Yao, S. Ping, MAO-DCPD composite coating on Mg alloy for degradable implant applications, Mater. Lett. 65 (2011) 2201–2204.
[32] J. Xu, I.S. Butler, D.F.R. Gilson, FT-Raman and high-pressure infrared spectroscopic studies of dicalcium phosphate dihydrate ($CaHPO_4 \cdot 2H_2O$) and anhydrous dicalcium phosphate ($CaHPO_4$), Spectrochim. Acta Part A 55 (1999) 2801–2809.
[33] W. Zhou, D. Shan, E.H. Han, W. Ke, Structure and formation mechanism of phosphate conversion coating on die-cast AZ91D magnesium alloy, Corros. Sci. 50 (2008) 329–337.
[34] J.M. Zhang, C.J. Lin, Z.D. Feng, Z.W. Tian, Mechanistic studies of electrodeposition for bioceramic coatings of calcium phosphates by an in situ pH-microsensor technique, J. Electroanal. Chem. 452 (1998) 235–240.
[35] N. Dumelie, H. Benhayoune, C. Rousse-Bertrand, S. Bouthors, A. Perchet, Characterization of electrodeposited calcium phosphate coatings by complementary scanning electron microscopy and scanning-transmission electron microscopy associated to X-ray microanalysis, Thin Solid Films 492 (2005) 131–139.
[36] Y. Huanga, Q. Dinga, X. Panga, S. Hana, Y. Yana, Corrosion behavior and biocompatibility of strontium and fluorine co-doped electrodeposited hydroxyapatite coatings, Appl. Surf. Sci. 282 (2013) 456–462.
[37] H.R. Bakhsheshi-Rad, M.H. Idris, M.R. Abdul-Kadir, Synthesis and in vitro degradation evaluation of the nano-HA/MgF_2 and DCPD/MgF_2 composite coating on biodegradable Mg–Ca–Zn alloy, Surf. Coat. Technol. 222 (2013) 79–89.
[38] Z. Shi, A. Atrens, An innovative specimen configuration for the study of Mg corrosion, Corros. Sci. 53 (2011) 226–246.
[39] M.A. Amin, M.M. Ibrahim, Corrosion and corrosion control of mild steel in concentrated H_2SO_4 solutions by a newly synthesized glycine derivative, Corros. Sci. 53 (2011) 873–885.
[40] X. Lin, L. Tan, Q. Zhang, et al., The in vitro degradation process and biocompatibility of a ZK60 magnesium alloy with a forsterite-containing micro-arc oxidation coating, Acta Biomater. 9 (2013) 8631–8642.
[41] S. Bose, S. Dasgupta, S. Tarafder, A. Bandyopadhyay, Microwave-processed nanocrystalline hydroxyapatite: simultaneous enhancement of mechanical and biological properties, Acta Biomater. 6 (2010) 3782–3790.
[42] P. Wan, X. Lin, L. Tan, et al., Influence of albumin and inorganic ions on electrochemical corrosion behavior of plasma electrolytic oxidation coated magnesium for surgical implants, Appl. Surf. Sci. 282 (2013) 186–194.
[43] H.M. Kim, T. Himeno, T. Kokubo, T. Nakamura, Process and kinetics of bonelike apatite formation on sintered hydroxyapatite in a simulated body fluid, Biomaterials 26 (2005) 4366–4373.
[44] M. Kheradmandfard, M.H. Fathi, M. Ahangarian, E.M. Zahrani, In vitro bioactivity evaluation of magnesium-substituted fluorapatite nanopowders, Ceram. Int. 38 (2012) 169–175.
[45] Z. Chun-Yan, Z. Rong-Chang, L. Cheng-Long, G. Jia-Cheng, Comparison of calcium phosphate coatings on Mg–Al and Mg–Ca alloys and their corrosion behavior in Hank′s solution, Surf. Coat. Technol. 204 (2010) 3636–3640.
[46] M.J. Jiao, X.X. Wang, Electrolytic deposition of magnesium-substituted hydroxyapatite crystals on titanium substrate, Mater. Lett. 63 (2009) 2286–2289.